

Original Article

Exploiting cell cycle inhibitor genes of the *KRP* family to control root-knot nematode induced feeding sites in plants

Roberta Ramos Coelho^{1,2†}, Paulo Vieira^{1,3†}, José Dijair Antonino de Souza Júnior^{1,2} , Cristina Martin-Jimenez¹, Lieven De Veylder^{4,5}, Julie Cazareth^{6,7}, Gilbert Engler¹, Maria Fatima Grossi-de-Sa² & Janice de Almeida Engler¹ 

¹INRA, University of Nice Sophia Antipolis, CNRS, UMR 1355-7254 Institut Sophia Agrobiotech, 06900 Sophia Antipolis, France, ²Embrapa Genetic Resources and Biotechnology, Parque Estação Biológica, PqEB – Av. W5 Norte, Caixa Postal 02372 CEP 70770-917 Brasília, DF, Brazil, ³NemaLab/ICAAM – Instituto de Ciências Agrárias e Ambientais Mediterrânicas, Universidade de Évora, Núcleo da Mitra, Ap. 94,7002-554 Évora, Portugal, ⁴Department of Plant Systems BiologyVIB, B-9052 Gent, Belgium, ⁵Department of Plant Biotechnology and Bioinformatics, Ghent University, B-9052 Gent, Belgium, ⁶Université de Nice Sophia Antipolis, 06103 Nice, France and ⁷Centre National de la Recherche Scientifique (CNRS), Institut de Pharmacologie Moléculaire et Cellulaire, UMR 7275, 06560 Valbonne, France

ABSTRACT

Cell cycle control in galls provoked by root-knot nematodes involves the activity of inhibitor genes like the *Arabidopsis* ICK/KRP members. Ectopic *KRP1*, *KRP2* and *KRP4* expression resulted in decreased gall size by inhibiting mitotic activity, whereas *KRP6* induces mitosis in galls. Herein, we investigate the role of *KRP3*, *KRP5* and *KRP7* during gall development and compared their role with previously studied members of this class of cell cycle inhibitors. Overexpression of *KRP3* and *KRP7* culminated in undersized giant cells, with *KRP3^{OE}* galls presenting peculiar elongated giant cells. Nuclei in *KRP3^{OE}* and *KRP5^{OE}* lines presented a convoluted and apparently connected phenotype. This appearance may be associated with the punctuated protein nuclear localization driven by specific common motifs. As well, ectopic expression of *KRP3^{OE}* and *KRP5^{OE}* affected nematode development and offspring. Decreased mitotic activity in galls of *KRP3^{OE}* and *KRP7^{OE}* lines led to a reduced gall size which presented distinct shapes – from more elongated like in the *KRP3^{OE}* line to small rounded like in the *KRP7^{OE}* line. Results presented strongly support the idea that induced expression of cell cycle inhibitors such as *KRP3* and *KRP7* in galls can be envisaged as a conceivable strategy for nematode feeding site control in crop species attacked by phytopathogenic nematodes.

Key-words: *Meloidogyne incognita*; *Arabidopsis*; giant cells.

INTRODUCTION

Root-knot nematodes (RKN) are economically important pathogens highly adapted for plant parasitism causing extensive damage to crops (Moens *et al.* 2009). Nematode-induced feeding sites (NFS) of the genus *Meloidogyne* are formed by specialized giant cells (GCs) within the root vascular cylinder, surrounded by proliferating neighbouring cells (NCs) (Huang

1985; Sijmons *et al.* 1994). Nematode secretions are most likely the inductive triggers to the dedifferentiation of vascular root cells into GCs (Rutter *et al.* 2014; Zhang *et al.* 2015). Induction of nematode feeding cells by RKN involves synchronous waves of mitotic activity with no cytokinesis. As GCs develop, their nuclei undergo multiple rounds of DNA synthesis along with increased cell size. The cell wall of these specialized feeding cells displays highly invaginated areas, resulting in the increased surface exchange with NCs and the xylem, allowing fast nutrient uptake (Huang 1985; Hoth *et al.* 2008; Rodiuc *et al.* 2014). The gall (or root-knot) is a result of the hyperplasia of NCs and the hypertrophy of GCs enfolding the nematode (Jones & Northcote 1972).

Root-knot nematodes are competent to locally alter plant gene expression (Gheysen & Fenoll 2002). Leaving the differentiated state is related to reentry into the cell cycle (De Veylder *et al.* 2007). Core cell cycle genes (such as *CDKA;1*, *CDKB1;1*, *CYCBI;1*, *CYCA2;1*, *CCS52* gene family, *DEL1*) of *Arabidopsis* are early induced during RKN parasitism and play essential roles during the formation of the NFS (Niebel *et al.* 1996; de Almeida Engler *et al.* 1999, 2011, 2012). The progression of the plant cell cycle is driven by the periodic activation of cyclin-dependent kinases (CDKs) that in combination with different cyclins (CYCs) trigger the transition of the different phases of the cell cycle (Inze & De Veylder 2006).

Plant genomes encode two plant-specific families of cyclin kinase inhibitors: the ICK/KRPs (interactors/inhibitors of CDK, also referred as Kip-Related Proteins) and the SIM/SMR (SIAMESE) families. Interactions of ICK/KRPs with CDK/CYCs complexes decrease CDK activity and affect both the cell cycle progression and DNA content in a concentration-dependent manner. In *Arabidopsis thaliana*, seven ICK/KRP members (hereafter mentioned as KRP) have been characterized which show distinct spatial and temporal expression patterns and exert distinctive functions (De Veylder *et al.* 2001; Menges & Murray 2002; Ormenese *et al.* 2004; Menges *et al.* 2005; Wang *et al.* 2006; Vieira *et al.* 2014). Both mitosis and endocycle share common molecular components. Normally, mitosis (G1, S, G2 and M phases) engages cell division,

Correspondence: J. de Almeida Engler. e-mail: janice.de-almeida@inra.fr

† Authors contributed equally to the work.

whereas endoreduplication (G1 and S phases) implies increased nuclear ploidy levels. It is therefore tempting to target both pathways to modulate progression of the cell cycle in GCs induced by RKN. Our previous studies have shown that *KRP2*, 5 and 6 are expressed in young GCs with distinct expression intensities during gall development (Vieira *et al.* 2013), whereas *KRP1*, 3, 4 and 7 showed no expression. *KRP2* knockout line revealed mild phenotypes with stimulated mitosis, whereas *kpr6* lines inhibited mitosis and stimulated cytokinesis resulting in frequent cell wall stubs between nuclei in GCs. Overexpression of the expressed *KRP2* as well as the expression of the not expressed *KRP1* and *KRP4* in GCs revealed that the increased levels of these proteins led to an inhibition of cell division and the endocycle consequently blocking the ordinary RKN life cycle (Vieira *et al.* 2012; Vieira *et al.* 2013). Unexpectedly, overexpression of the *KRP6* protein rather stimulated mitosis in GCs and NCs, but still inhibiting giant-feeding cells expansion and nematode development, most likely due to the consequent delay in the endocycle (Vieira *et al.* 2014). The mitotic stimulation under ectopic *KRP6* expression induced additional multinucleation in GCs inhibiting cytokinesis (Vieira *et al.* 2014; Vieira & de Almeida Engler 2015). Therefore, *KRP6* expression in GCs has been accounted for inducing multinucleation in GCs and contributing for cytokinesis arrest.

Having observed diverse functions amongst the different *KRP* family members formerly analysed during gall development, herein we explore the effect of ectopic expression of the expressed *KRP5* in GCs and compared to the ectopic expression of *KRP3* and *KRP7* genes, which are absent during gall development in *Arabidopsis*. Overexpression of *KRP3*, 5 and 7 on galls resulted in different levels of inhibitory effects leading to a disarray of the cell cycle, later affecting RKN reproduction and offspring.

MATERIALS AND METHODS

Plant growth and transformations

KRPpro:GUS (*KRP3*, *KRP5* and *KRP7*) lines were generated as described by Vieira *et al.* (2013). The intergenic regions (up to maximum 2 kb) were amplified from *A. thaliana* genomic DNA. The corresponding PCR fragments were cloned into the pDONR207 entry vector by BP recombination cloning and subsequently transferred into the pKGWFS7 destination vector (Karimi *et al.* 2002) by LR cloning, resulting in a transcriptional fusion between the *KRP* promoters and the *EGFP-GUS* fusion gene. The loss-of-function *kpr5* mutant lines (Salk-053533 and Salk-0897170) were obtained from the *Arabidopsis* Biological Resource Center. Homozygous knock-out mutant lines were tested by PCR with specific primers using genomic DNA (Supporting Information Table S1). Kanamycin-resistant T3 overexpressing lines of the three *KRP* genes, namely *35S:KRP3-GFP*, *35S:GFP-KRP5* and *35S:KRP7-GFP* (hereafter referred to as *KRP3^{OE}*, *KRP5^{OE}* and *KRP7^{OE}*, respectively), were bulked and selected from T0 lines kindly provided by Eugenia Russinova. *Arabidopsis thaliana* genotype Columbia 0 (Col-0) was used as the wild-type control. Both transgenic and wild-type *A. thaliana* Col-0

seeds were surface sterilized for 5 min in 5% NaOCl, washed four times with 95% ethanol and dried under the hood overnight. Seeds were germinated and grown in a growth chamber with a 16 h light/8 h dark photoperiod at 21 °C/18 °C, respectively.

In vitro grown seedlings and nematode infection

Arabidopsis thaliana seeds were surface sterilized, dried and germinated on Murashige and Skoog germination medium (Duchefa, Haarlem, the Netherlands) containing 1% sucrose and 0.8% plant cell culture-tested agar (Daichin) and subsequently kept in the fridge for 48 h to synchronize germination. Plantlets were kept inclined allowing roots to grow at the surface for 7 d and then transferred to KNOP medium (Sijmons *et al.* 1991) to stimulate root growth. To generate galls *in vitro*, pre-parasitic juvenile nematodes were sterilized with 0.01% HgCl₂ for 10 min passing through a support holding a sterile paper filter. Subsequently, nematodes were treated with 50 mg L⁻¹ kanamycin for 5 min and washed three times with sterile water. Sterile juveniles were then collected from the filter in sterile water, counted and immediately used for infection of transgenic *Arabidopsis* seedlings. Approximately 100 sterile juveniles were used for infection per plant.

GUS histochemical analysis and microscopy

GUS activity driven by *KRP3*, *KRP5* and *KRP7* gene promoters was monitored at 3, 7, 14, and 21 d after inoculation (DAI), as described by de Almeida Engler *et al.* (1999), using 200 *Meloidogyne incognita* freshly hatched second-stage juveniles as nematode inoculum for each individual plant. Whole galls were fixed and infiltrated with a chloral-lactophenol clearing solution (Beeckman & Engler 1994) for examination with differential interference contrast bright-field optics. For dark-field microscopy, gall samples were fixed overnight in 2.0% glutaraldehyde and embedded in Technovit 7100 (Heraeus Kulzer) as described by the manufacturer and semi-thin sectioned (3 µm) using standard microtomy described by de Almeida Engler *et al.* (2012).

RT-PCR analyses of transgenic versus wild-type lines

To confirm the respective absence of transcripts in *kpr5* mutant lines (Salk-053533 and Salk-0897170), or the *KRP* levels in overexpressing lines (*KRP3^{OE}*, *KRP5^{OE}* and *KRP7^{OE}*), semi-quantitative RT-PCR was performed. Total RNA was extracted with RNeasy Plant Mini Kit (Qiagen) according to the manufacturer's instructions from 7-day-old whole seedlings. cDNA synthesis was performed using the SuperScript III First-Strand Synthesis System for RT-PCR. Plants overexpressing each *KRP* gene (*KRP3^{OE}*, *KRP5^{OE}* and *KRP7^{OE}*) were selected based on their respective gene expression levels, phenotype and protein localization. Pairs of primers used for *kpr5* loss-of-function validation and for all overexpressing lines are specified in Supporting Information Table S1.

Morphological analysis of gall tissues

Arabidopsis thaliana wild-type Col-0 seeds and transgenic lines were germinated as described by de Almeida Engler *et al.* (1999) supplemented with the proper antibiotics. Three-week-old seedlings of overexpressing and knockout lines, and respective controls, were then transferred to soil as described by de Almeida Engler *et al.* (2016) and 10 d later infected with 200 freshly hatched *M. incognita* second-stage juveniles. Infected roots were harvested at 7, 14, 21 and 40 DAI and fixed and embedded as described for GUS analysis. Galls were sectioned (3 µm), stained in 0.05% toluidine blue and mounted in DPX (Sigma-Aldrich). Microscopy analyses were carried out using bright-field optics, and images were acquired with a digital camera (Axiocam, Zeiss).

Surface measurement of giant cells

Up to three of the largest GCs per gall section of nematode-infected *KRP3^{OE}* and *KRP5^{OE}* roots were selected and analysed for the different stages after nematode infection (7, 14, 21 and 40 DAI), and surface measured using the Axioplan software (Zeiss). A minimum of 30 GCs were measured for *KRP3^{OE}* and *KRP5^{OE}* from root sections from each time point studied. Considering the low gall number observed in the *KRP7^{OE}* line, GC dimensions were recorded for only one time point (21 DAI). For the *KRP3^{OE}* and *KRP5^{OE}* lines, the effect of the overexpression at four time points was evaluated by analysis of variance, using the SPSS software (version 10, Chicago, IL).

Whole-mount analysis of 4,6-diamidino-2-phenylindole stained and cleared galls

4,6-Diamidino-2-phenylindole (DAPI) staining of nuclei in cleared galls was performed and analysed as described by Antonino de Souza Junior *et al.* (2016). DAPI stained samples were mounted in 90% glycerol on microscope slides. Cleared galls were imaged using a Leica SP8 confocal microscope with objective lens HC PL APO CS1 40X/1.30 OIL. Dye excitation was done with a diode 405 nm laser and fluorescence was collected between 431 and 532 nm. All samples were scanned at 400 Hz and 16X line averaged for high quality image recording. Z-stacks were generated from approx. 100 images with a 1 µm optical slice thickness and used to generate maximum brightness projections.

Volumetric measurements of giant cell nuclei

Volumetric measurements of nuclei in GCs of *KRP7^{OE}* line were performed. Imaged stacks of DAPI-stained galls were analysed with the ImageJ software. The nuclear volume was measured using the plug-in Volumest that allows estimating volumes of confocal data sets. A total of 164 nuclei were measured in *KRP7^{OE}* galls and 431 nuclei in wild-type.

Flow cytometry analyses of infected and gall-less roots

Nuclear flow cytometry of galls was performed as described by Vieira *et al.* (2013). The nuclei were examined with the LSRII Fortessa (BD Biosciences) flow cytometer and the BD FACS Diva software (BD Biosciences). For uninfected and gall-less roots, data were assembled from approximately 2000 nuclei per run. For *KRP3^{OE}* and *KRP5^{OE}*, ploidy levels of 40 galls (30 DAI) were pooled for each independent biological repetition (two in total), while for *KRP7^{OE}* only one repetition was analysed. Two replicates were carried out per biological repetition for each line, and data of approximately 40 000 nuclei per run were collected. The mean values of repetitions of the two independent experiments were calculated, and the portion of nuclei with ploidy levels from 2C to 128C was expressed as the percentage of the total number of nuclei recorded.

KRP protein localization during cell division in root meristem cells and nematode feeding sites

Whole non-infected 7-day-old roots of *KRP3^{OE}*, *KRP5^{OE}* and *KRP7^{OE}* lines were examined using an inverted confocal microscope (ZEISS LSM510 META) for KRP protein localization during cell division. The *KRP* overexpressing lines were then inoculated with sterile *M. incognita* as described above and galls at 14 and 21 DAI were dissected from roots and mounted in 5% agar. Thick gall slices of 100–200 µm were made with a HM650V Vibratome Microm (Walldorf, Germany) and immediately analysed by confocal microscopy. Specific GFP fluorescence was confirmed by spectral imaging using 488 nm laser line excitation and emission spectrum acquisition between 499 and 550 nm. Alternatively, GFP emission fluorescence was captured in standard scanning mode with a 500–530 nm band pass emission filter. In addition, to evaluate if the KRP5 protein was degraded by the anaphase promoting complex in galls, the GFP fluorescence was analysed in *35S:GFP-KRP5* transgenic plants treated with the 26S proteasome inhibitor MG132 (Sigma-Aldrich) and compared to untreated galls. Galls were treated with 100 µM MG132 (10 mM were dissolved in DMSO and diluted to 100 µM with water) for 6 h, and fresh gall slices were analysed by confocal microscopy.

Nematode infection tests and acid fuchsin staining

Three-week-old *A. thaliana* Col-0 and transgenic seedlings germinated *in vitro* were transferred to soil and 10 d later infected with 200 freshly hatched *M. incognita* second-stage juveniles (de Almeida Engler *et al.* 2016). Thirty days after inoculation, the number of galls and egg masses from each plant were counted and compared with control plants. Infection tests for each transgenic line were performed for two independent biological repetitions. To identify stages of nematode development and egg masses associated with galls, infected roots were fixed and stained with acid fuchsin as described by Vieira *et al.* (2014).

RESULTS

Promoter activity of *KRP3*, *KRP5* and *KRP7* genes in galls

Promoter activity was monitored in detail during various gall developmental stages and confirmed no GUS activity of

KRP3 or *KRP7*, and high *KRP5* promoter activity early after infection (3–7 DAI) which decreased in mature galls (21 DAI; Supporting Information Fig. S1) using short GUS-staining incubations (1 h). Longer incubation times (ON) of *KRP3pro:GUS* and *KRP7pro:GUS* lines showed very weak punctual GUS activity at comparable time points during gall

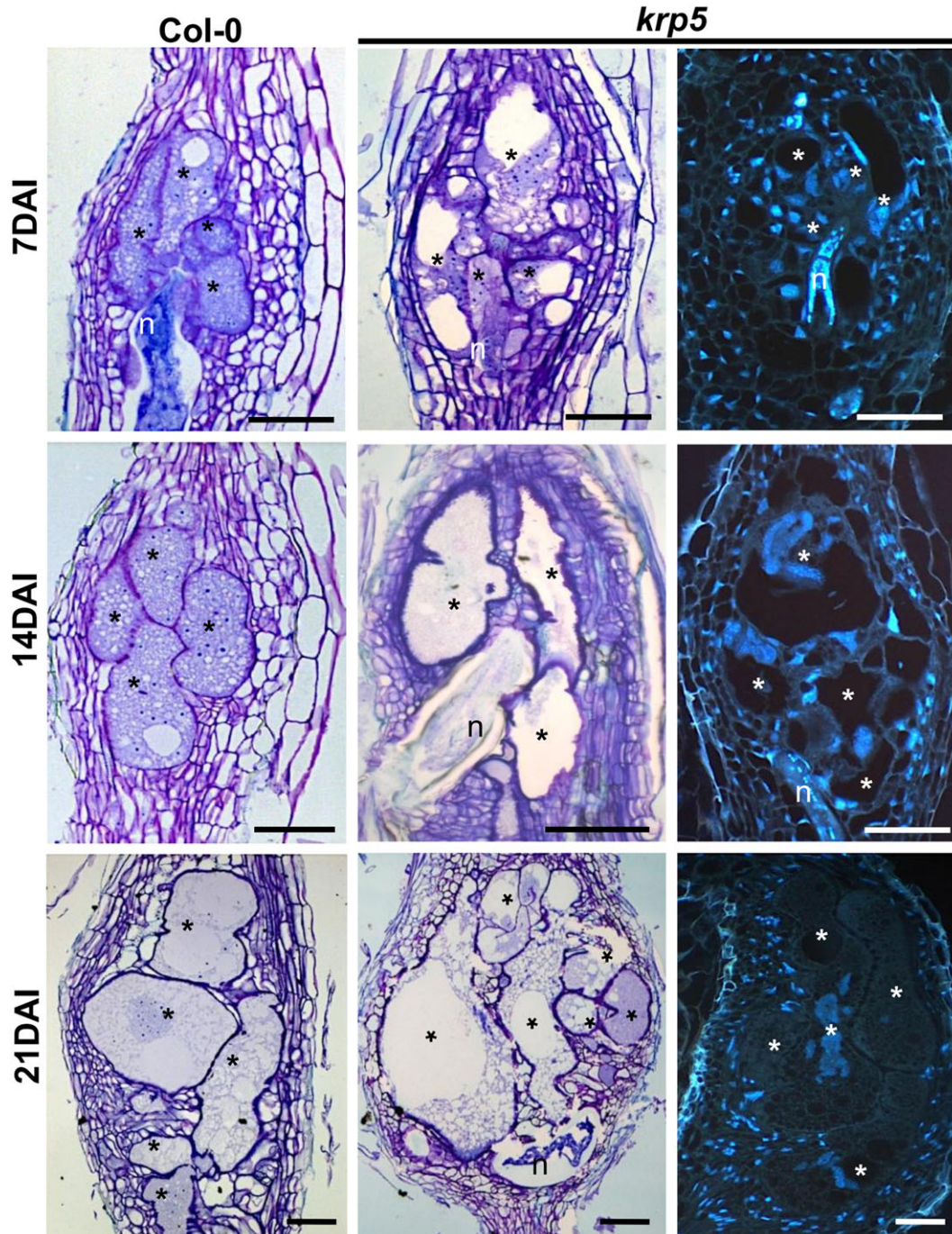


Figure 1. Histological analysis of gall tissues in the *krp5* line of *Arabidopsis* upon infection with *Meloidogyne incognita*. Bright-field images of longitudinal sections of galls stained with toluidine blue in wild-type and *krp5* mutant at different stages of nematode infection [7, 14 and 21 d after inoculation (DAI)]. Less cytoplasm was observed in nematode induced giant cells. Asterisk, giant cell; n, nematode. Bars = 50 μ m.

development (Supporting Information Fig. S1), suggesting the absence of expression of these two cell cycle inhibitors in nematode-induced galls.

Loss of *KRP5* function affects nematode reproduction

Considering that *KRP5* gene was the only member here analysed showing expression in galls, we used single insertion mutant lines of *krp5* for a detailed morphological analysis of the NFS development. Gall morphology in both *krp5* knockout lines was alike to the wild-type at early time points, but at later time points (14 and 21 DAI) GCs contained less cytoplasm and larger vacuoles (Fig. 1), possibly causing a delay on nematode development. DAPI stained nuclei in the *krp5* line showed that mitotic activity and DNA replication occurred in GCs seen by the nuclei phenotype at 7 to 21 DAI (Fig. 1). Nuclei number often seemed higher than in wild-type galls (Fig. 1 *krp5* 7DAI). Infection tests were focused on one *krp5* (SALK-053533) mutant line (Supporting Information Fig. S2), and data showed a significant reduction of egg masses (approx. 45% less egg masses than wild-type) (Fig. 2a). Acid fuchsin stain revealed a delay in nematode development (Fig. 2b), with fewer females containing associated egg masses in comparison to wild-type galls (Fig. 2a).

Overexpression of *KRP3*, *KRP5* and *KRP7* differentially affects gall development

In order to evaluate the ectopic effects of *KRP3*, *5* and *7* genes in galls, overexpressing lines (*35S:KRP3-GFP*, *35S:GFP-KRP5* and *35S:KRP7-GFP*) were generated and analysed during gall development. Lines selected for RKN infection were based on three criteria: presence of the typical serrated leaf phenotype denoting inhibition of cell proliferation (Supporting Information Fig. S3a); increased expression levels of the *KRP* gene

(Supporting Information Fig. S3b); and exclusive nuclear localization of the corresponding protein (Supporting Information Fig. S3c) also validated the functionality of overexpressing lines.

A detailed microscopy analysis of NFS induced in both *KRP3^{OE}* and *KRP7^{OE}* roots illustrated a severe reduction of gall size at different developmental stages (7, 14, 21 and 40 DAI) as a result of the reduced GC dimensions (Supporting Information Fig. S4a,c) and decreased cell division of surrounding NCs (Fig. 3). Distinctively, galls induced in the *KRP3^{OE}* line showed exceptionally narrowed phenotype of GCs (Fig. 3). In the *KRP7^{OE}* line, galls and GCs were obviously smallest, while the reduced number of NCs presented a disorganized morphology (Fig. 3). Galls formed in the *KRP5^{OE}* background were also smaller due to decreased NC division compared to controls (Fig. 3).

Surface measurements were carried out on GC sections for lines of the three overexpressing genes and compared to the size of wild-type GCs (Supporting Information Fig. S4). The average surface of GCs in the *KRP3^{OE}* line was significantly smaller than in wild-type even when cells were elongated (Supporting Information Fig. S4a). Although galls induced in the *KRP5^{OE}* were frequently smaller, the variability in GC surface size did not show statistical differences amongst the different time points studied (Supporting Information Fig. S4b). Differently, in the *KRP7^{OE}* line, smaller rounded GCs (Supporting Information Fig. S4c) and repressed NC division resulted in galls with reduced size compared to wild-type.

Ectopic *KRP* expression induces nuclear changes in giant cells

Morphological analyses by confocal microscopy of thick gall sections cleared and DAPI-stained of the three *KRP^{OE}* lines revealed major changes in size, number and shape of GCs nuclei. Three-dimensional confocal projections of serial optical sections of galls at 7, 14 and 21 DAI for each *KRP^{OE}* lines were

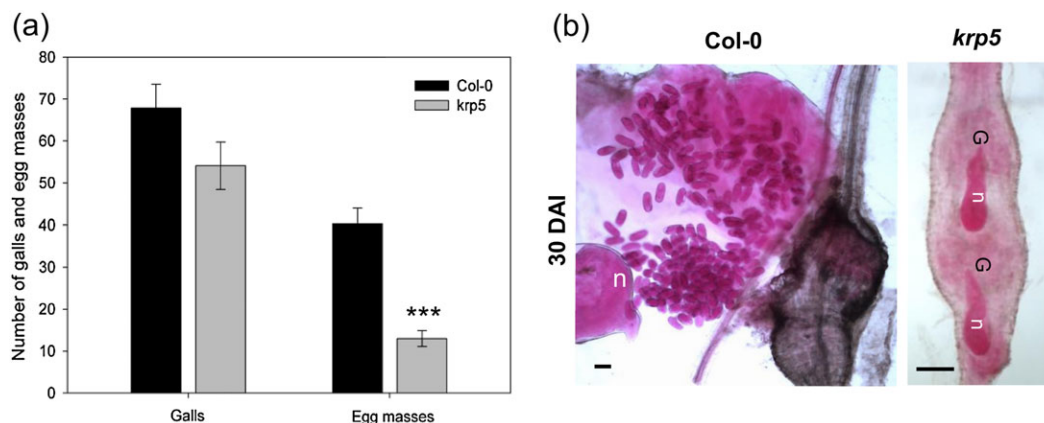


Figure 2. Nematode infection tests and development in the *krp5* line compared to the wild-type. (a) Nematode infection tests of the *krp5* line compared to the wild-type Col-0. Data shown represents means \pm SE from two independent biological repetitions, in which a minimum of 30 seedlings of each line were evaluated for nematode infection in soil. Pairwise comparisons were made by Student's *t*-test ($P \leq 0.05$). (b) Acid fuchsin staining of galls at 30 DAI. In most *krp5* galls, the females have not reached maturity and consequently did not produce eggs. e, eggs; G, gall; n, nematode. Scale bars = 50 μ m.

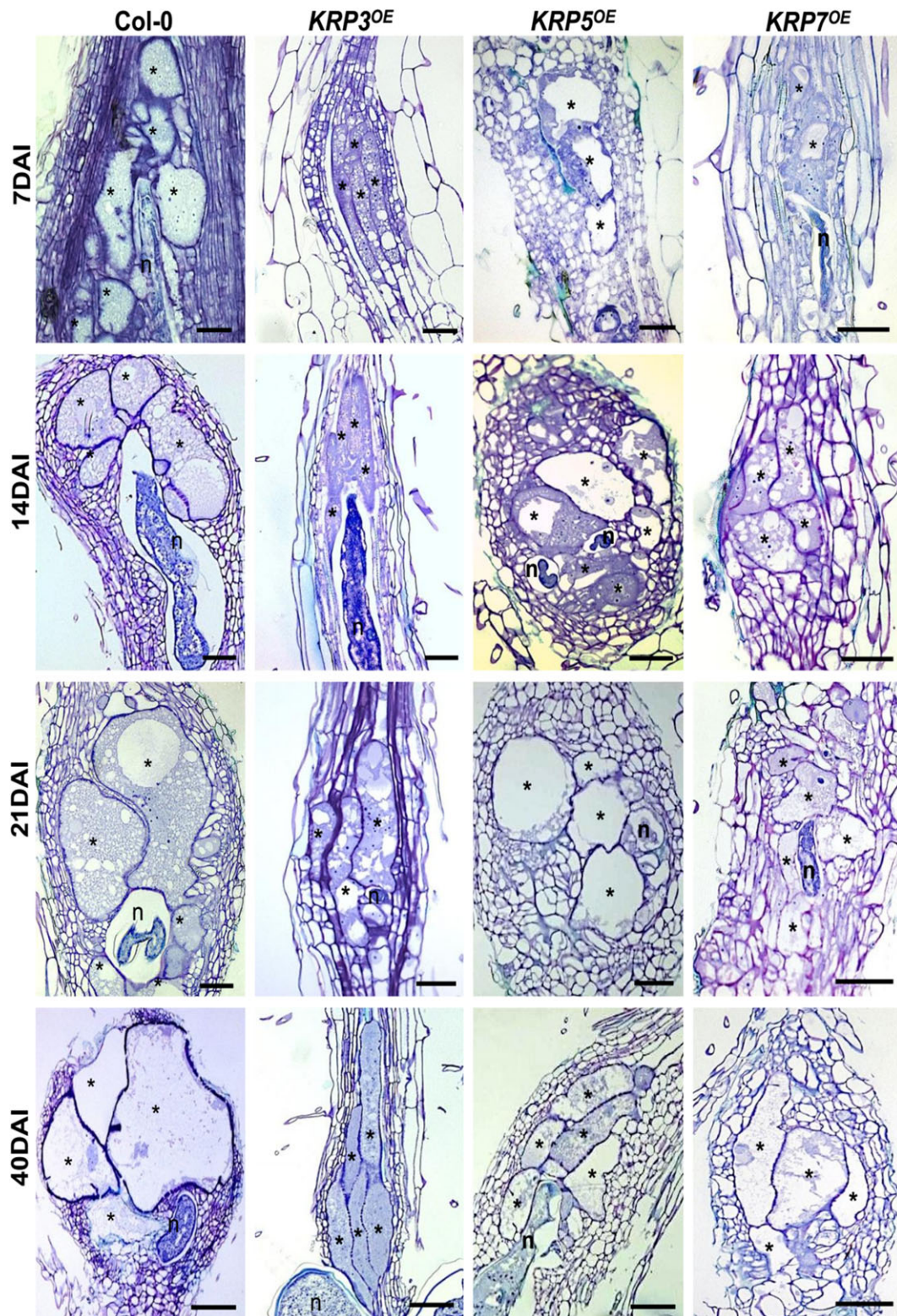


Figure 3. Ectopic *KRP* expression significantly affects the size of galls induced by *M. incognita*. Histological analysis of nematode-induced wild-type galls compared to *KRP3*^{OE}, *KRP5*^{OE} and *KRP7*^{OE} lines at different phases of nematode infection (7, 14, 21 and 40 DAI). Bright-field images of longitudinal gall sections stained with toluidine blue. Note that in lines with ectopic *KRP3* expression giant cells are elongated and the number of neighbouring cells is significantly reduced. Asterisk, giant cell; n, nematode. Scale bars = 50 μm.

generated and compared with those of the wild-type (Fig. 4). Giant cells within the *KRP3^{OE}* line displayed prominent elongated nuclei, which were apparently connected as gall developed, suggesting a cumulative effect of mitotic defects within the GCs (Fig. 4a–c; Supporting Information Movie S1). Similarly, but less frequent, an elongated nuclear phenotype was also observed in GCs within the roots of the *KRP5^{OE}* line (Fig. 4d–f and Supporting Information Movie S2). Differently, GCs in *KRP7^{OE}* line presented fewer and rounded nuclei (Fig. 4g and Supporting Information Movie S3), compared to wild-type (Fig. 4h and Supporting Information Movie S4), in

contrast to the elongated and connected nuclei observed in both *KRP3^{OE}* and *KRP5^{OE}* lines.

Ectopic *KRP3* expression induces changes in nuclei shape and ploidy levels in giant cells

Due to the convoluted, elongated and variable sizes of the clustered nuclei within *KRP3^{OE}* and *KRP5^{OE}* GCs (Fig. 5c,f), it was not possible to accurately record the average number of nuclei and measure nuclei surfaces associated within each GCs.

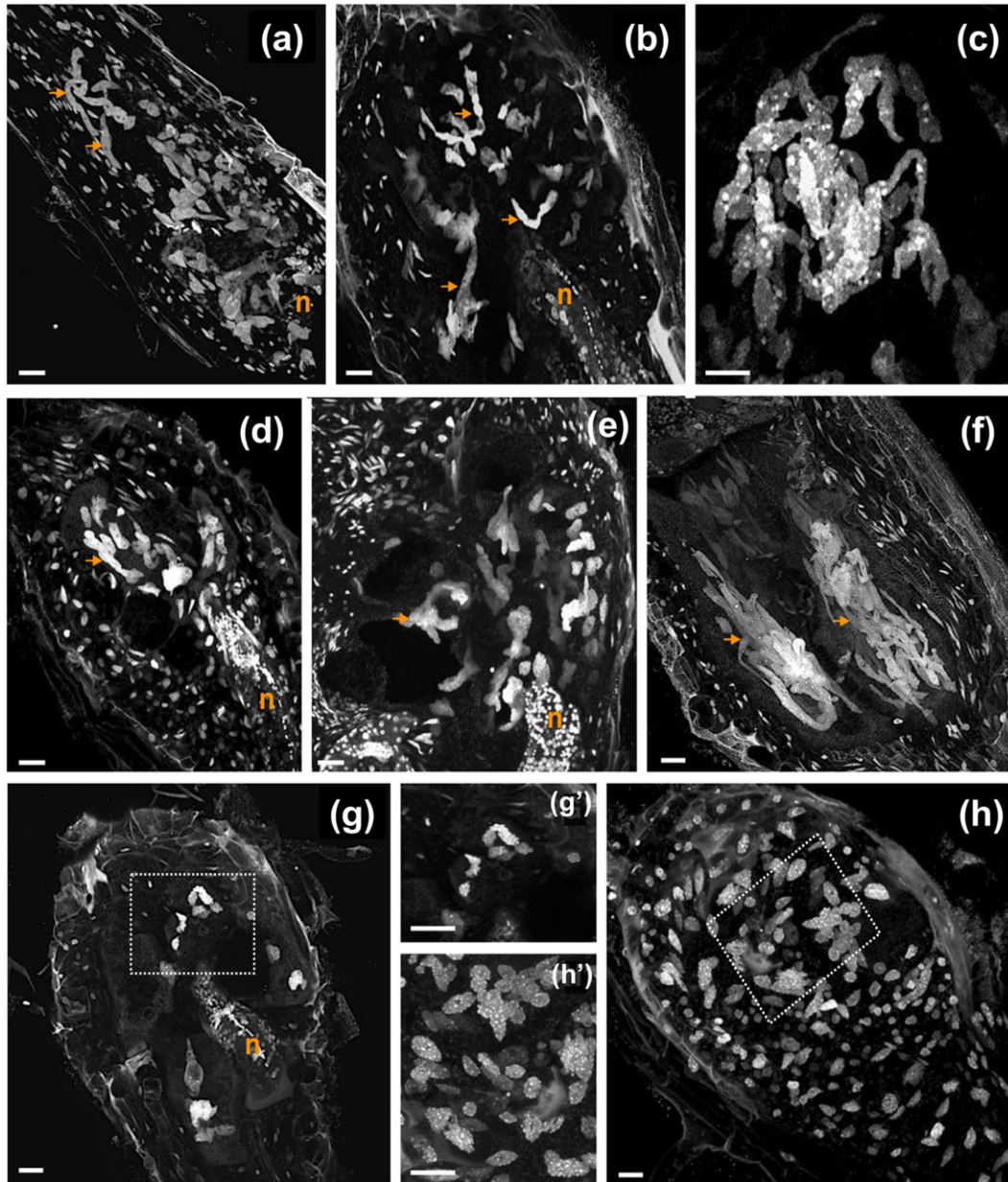


Figure 4. Ectopic *KRP3*, *KRP5* and *KRP7* expression causes nuclear morphology changes in giant cells. (a–h) 3D confocal projection of serial optical sections of thick slices cleared and stained with DAPI allowed the visualization of changes of nuclear morphology in mutant lines. (a–c) *KRP3^{OE}* gall 7, 14 and 21 DAI. (d–f) *KRP5^{OE}* gall 7, 14 and 21 DAI. (g) *KRP7^{OE}* gall 21 DAI. (h) Wild-type gall 21 DAI. Elongated nuclei apparently connected are observed already early (7 DAI, orange arrows) in giant cells of *KRP3^{OE}* and *KRP5^{OE}* lines. Scale = 50 μ m. [Colour figure can be viewed at wileyonlinelibrary.com]

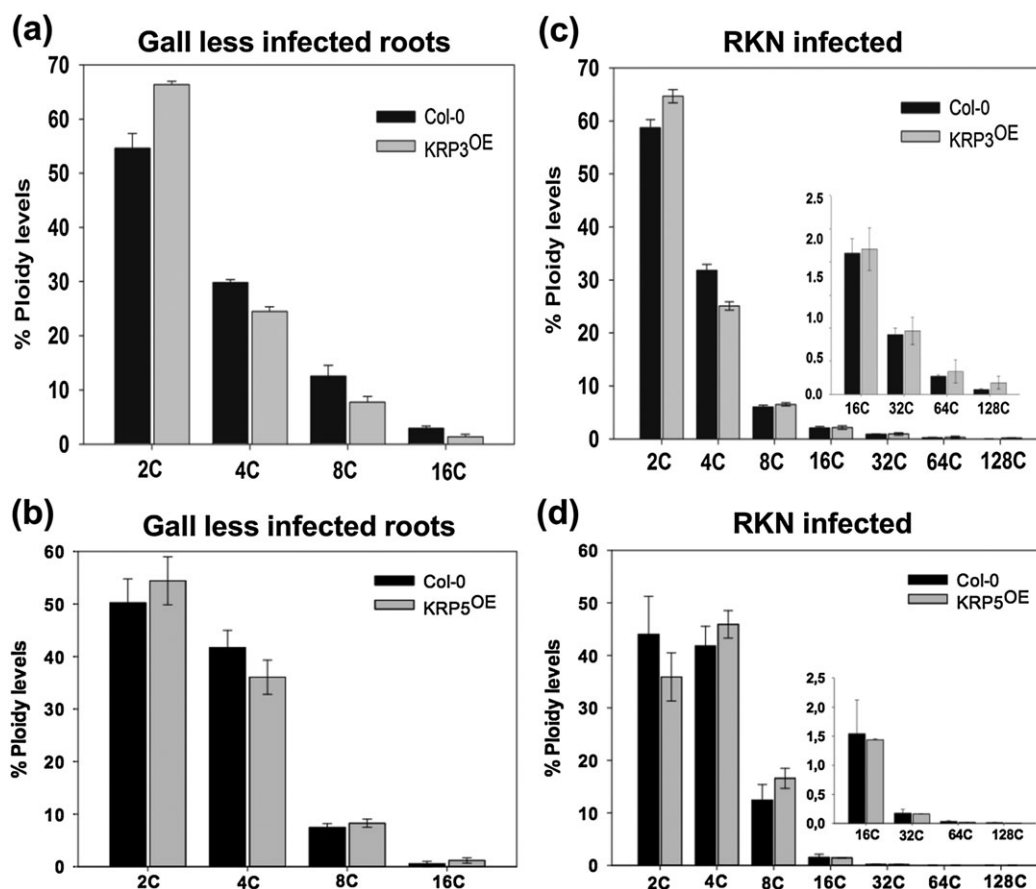


Figure 5. Nuclear flow cytometry analysis of roots and galls ectopically expressing *KRP3* and *KRP5*. (a–b) Percentage of ploidy levels of nuclei in gall-less wild-type roots in the *KRP3*^{OE} (a) and *KRP5*^{OE} (b) lines. (c–d) Percentage of ploidy levels in galls (30 DAI) in the *KRP3*^{OE} (c) and *KRP5*^{OE} (d) lines. In *KRP3*^{OE}, an increase in nuclei with high ploidy levels was observed at 16C to 128C, while in *KRP5*^{OE}, nuclear ploidy levels were higher only for 4C and 8C compared to wild-type galls.

However, the enlarged nuclei at early time points after infection (7 DAI) in both *KRP3* and 5 overexpressing lines suggest that these nuclei may enter the endoreduplication cycle earlier (Fig. 5a,d). Therefore, nuclear flow cytometry measurements were performed for roots and galls. Results revealed that the ploidy levels of gall-less roots of wild-type and mutant lines ranged from 2C to 16C (Fig. 6a,b). Ploidy populations from wild-type galls varied from 2C to 128C (Fig. 6c,d). In the *KRP3*^{OE} line, we could observe a slightly increased ratio of nuclei over 8C to 128C compared to wild-type galls (Fig. 6c). For the *KRP5*^{OE} line, nuclear ploidy levels of GCs showed only small differences amongst nuclei containing 4C and 8C (Fig. 6d). No clear differences in GCs ploidy levels might be due to the elongated nuclei phenotype observed for both *KRP3*^{OE} and *KRP5*^{OE} lines.

A single flow cytometric measurement was performed for *KRP7*^{OE} line due to the very low gall number per seedling (Fig. 7a). Results suggested that higher ploidy levels are present in GCs overexpressing *KRP7*. Volumetric measurements of nuclei in GCs in the *KRP7*^{OE} line showed that the total nuclei volume was higher in wild-type GCs considering the higher nuclei number (Fig. 7b,c). However, the range of nuclei average volume values showed to be higher in *KRP7*^{OE} line than in wild-type (Fig. 7d), suggesting that the cells tried to

compensate the low number of nuclei in *KRP7*^{OE} by generating larger nuclei by promoting the endocycle. This observation corroborated with flow cytometric measurements where higher ploidy levels were observed in *KRP7*^{OE} GC nuclei.

KRP protein localization in uninfected roots and galls

All KRPs *Arabidopsis* members show a strict nuclear localization during interphase, with *KRP3*-GFP and GFP-*KRP5* displaying a sub-nuclear localization (Supporting Information Fig. S3c). Herein, we report the subcellular localization of *35S:KRP3-GFP*, *35S:GFP-KRP5* and *35S:KRP7-GFP* in root cells during mitosis by time-lapse confocal microscopy (Fig. 7). For *KRP3*-GFP and GFP-*KRP5*, we observed protein colocalization with chromosomes in mitotic dividing cells, from anaphase to the following stages of mitosis (Fig. 7), while *KRP7*-GFP became dispersed into the cytoplasm after nuclear envelope breakdown. Throughout mitosis, a weak *KRP7* fluorescence was observed within the cytoplasm, and during cytokinesis, a progressive accumulation of *KRP7* could be observed in the nuclei of the two new daughter cells (Fig. 7). Protein localization of the three KRPs was followed *in vivo* during

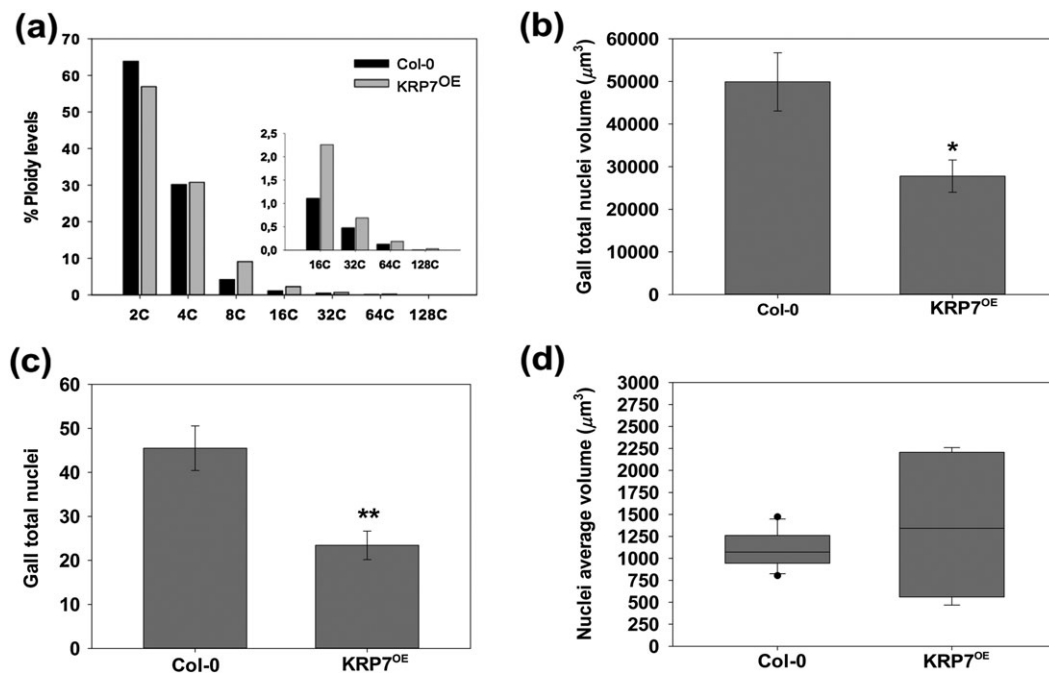


Figure 6. Nuclei volume of *KRP7^{OE}* galls compared with wild-type. (a) Nuclear flow cytometry analysis of galls in the *KRP7^{OE}* line and wild-type lines. Although few nuclei were present within giant cells (less mitotic events), the number of nuclei with increased ploidy levels (stimulated endocycle) were higher than in wild-type. (b) Total volume of nuclei in giant cells per gall. (c) Average number of nuclei per grouped giant cells. (d) Nuclei average volume in grouped giant cells in galls. The distribution is shown by vertical box plot. The lines within the boxes indicate the average of nuclei volumes, and the upper and lower box edge indicates variation of 25 to 75%. The bars show the largest/smaller values of average volumes that fall within a distance of 1.5 times interquartile range (IQR) from the upper and lower hinges, and the dots are the values that fall outside the IQR. Statistical differences are marked with * ($P < 0.05$) or ** ($P < 0.01$) based on Student's *t*-test analysis.

NFS development. 3D-confocal projections confirmed the elongated GCs nuclei for the *KRP3^{OE}* line (Supporting Information Fig. S4a,b), as observed in DAPI-stained cleared galls (Fig. 5a–c). As well, *in vivo* *KRP7*-GFP line illustrated sparse and enlarged nuclei (Supporting Information Fig. S5c,d). Our data suggests that the co-localization of *KRP3* and *KRP5* proteins within the chromosomes could be related to an erroneous segregation of chromosomes causing connectivity of the GC nuclei when these genes are overexpressed.

Treatment with the proteasome inhibitor MG132 increases GFP-KRP5 protein levels in galls

To investigate if GFP-KRP5 was regulated by the 26S proteasome protein degradation in roots and gall cells, we applied the inhibitor MG132. Expression of the GFP-KRP5 fusion protein was clearly increased in uninfected roots (Fig. 8a) as well as in galls upon MG132 treatment (Fig. 8c) compared to untreated samples (Fig. 8b,d). This accumulation of GFP-KRP5 suggests that *KRP5* protein is targeted by the proteasome for degradation in galls.

Ectopic expression of *KRP* impairs nematode maturation and reduces offspring

We also examined the effect of the ectopic expression of *KRP3*, 5 and 7 would have any effect on the nematode life

cycle. In the three *KRP^{OE}* lines, infective J2 nematodes were able to penetrate and migrate along the roots, and induce galls. However, at 30 DAI, a 40 to 80% reduction in gall number was observed (Fig. 9a–c) compared to wild-type. Reduction in egg mass number was also observed for the *KRP3^{OE}* and *KRP5^{OE}* lines (Fig. 9a,b), whereas at this time point, no egg masses were yet detected in the *KRP7^{OE}* line (Fig. 9c).

Infected roots (30 DAI) were then stained with acid fuchsin to evaluate the developmental stage of the nematodes associated with each gall (Fig. 9d). Whereas in wild-type plants, most of the pear-shaped females achieved the reproductive maturity, including well-developed egg masses, in the three *KRP* overexpressing lines, most nematodes associated with these galls were under-developed compared to wild-type (Fig. 9d).

DISCUSSION

Successful parasitism of obligatory sedentary plant-pathogens such as the RKN is dependent on the cell cycle machinery of the plant host (de Almeida Engler *et al.* 2011). Previously, we have shown that ectopic expression of *KRP1*, *KRP2* and *KRP4* severely reduced gall expansion by decreasing GC size and inhibiting NC division (Vieira *et al.* 2012, 2013). Conversely, overexpression of *KRP6* accelerated gall mitotic activity resulting in the formation of large galls filled with NCs but containing GCs of reduced size (Vieira *et al.* 2014). These data

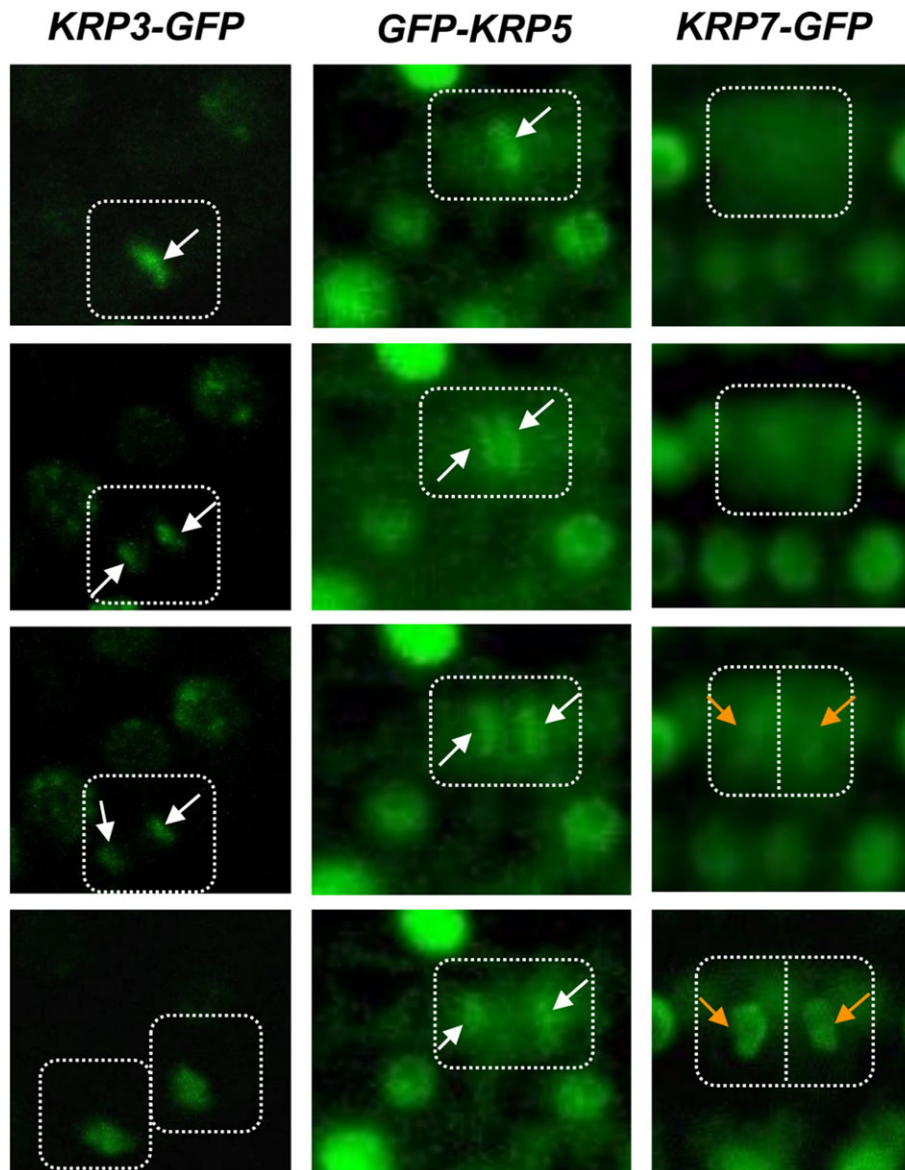


Figure 7. KRP3-GFP, GFP-KRP5 and KRP7-GFP localization in *Arabidopsis* during cell division, using 7-day-old seedlings. Time lapse during mitotic cell division in *Arabidopsis* root cells. White arrows point to co-localization of KRP3-GFP and GFP-KRP5 with chromosomes, and orange arrows points to the progressive accumulation of KRP7-GFP in the two daughter cells nuclei, respectively.

demonstrate that different members of the *Arabidopsis* ICK/KRP family can exert different functions and effects during gall development. KRPs interact with CDKA;1 and form complexes with D-type cyclins (De Veylder *et al.* 2001; Verkest *et al.* 2005; Boruc *et al.* 2010; Van Leene *et al.* 2010, 2011). KRP5 appear to bind preferentially to distinct CDK–cyclin complexes, like CYCD2;1, CYCD4;1 and CYCD4;2. In addition, different KRPs do not inhibit the kinase activity of the CDKA complex *in vitro* with the same efficiency (Wang *et al.* 1997) justifying their distinct actions. Therefore, we investigated how the ectopic expression of the three remaining KRP genes (*KRP5* expressed, and *KRP3* and *KRP7* not expressed in galls) of *A. thaliana* might affect NFS development.

***KRP3*, *KRP5* and *KRP7* are differently expressed in galls**

Promoter-GUS fusions and mRNA *in situ* hybridization have shown the *KRP5* expression in galls, while transcripts of *KRP3* and *KRP7* were not detected (Vieira *et al.* 2013). Here, we show in detail that the *KRP5* promoter activity increases during GC induction (1 to 7 DAI) and expansion (up to 14 DAI). *KRP5* is highly expressed in endoreduplicating plant cells, as for expanding GCs, and is required to induce endocycles in etiolated seedlings (Jégu *et al.* 2013). Absence of *KRP3* or *KRP7* expression in nematode feeding sites follows similar expression profiles observed in uninfected root vascular tissues. These observations differ from promoters of other cell

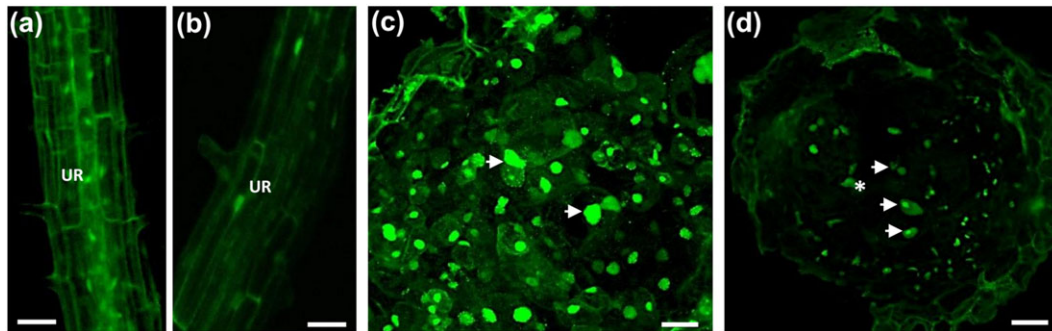


Figure 8. Increased GFP fluorescence in nuclei of roots and giant cells in the *KRP5^{OE}* line was observed upon treatment with the proteasome inhibitor MG132. (a–d) *In vivo* localization of GFP-KRP5 (green) in nuclei of an uninfected root (a,b) and galls 14 DAI (c,d) respectively. GFP-KRP5 localization in nuclei of (a,c) treated and (b,d) untreated roots and galls 14 DAI, respectively. Note the increased fluorescence on MG132-treated roots and galls. Scale bars = 25 μ m.

cycle genes like *CYCB1;1* which is early induced in galls and absent in the vascular cylinder, location of nematode feeding site induction (de Almeida Engler *et al.* 1999).

***KRP5* loss-of-function moderately affects giant-feeding cell development**

Morphological analysis of galls induced in the *kpr5* loss-of-function lines showed mild defects caused by *KRP5* deficiency as observed in *Arabidopsis* seedlings (Jégu *et al.* 2013). The lack of a drastic phenotype might be caused by a redundant function of *KRP5* with other *KRPs* expressed in galls (Vieira *et al.* 2013). Nevertheless, absence of *KRP5* delayed nematode maturation and reproduction possibly due to the more frequent presence of vacuoles in GCs, suggesting fewer nutrients available.

Ectopic *KRP* expression influences giant cell and nuclei shape and affects ploidy levels in feeding sites

KRP3^{OE}, *KRP5^{OE}* and *KRP7^{OE}* lines generated herein were challenged by *M. incognita*. Ectopic *KRP5* expression appears not to affect drastically the overall gall or GC morphology, or cell division, but prevents cells to progress into the cell cycle, as observed in lateral roots by Jégu *et al.* (2013). Cell cycle inhibition in the *KRP5^{OE}* line was enough to cause an overall decrease in gall and egg mass number, even when suggested by Jégu *et al.* (2013) that *KRP5* inhibits cell proliferation with a lower efficiency than other *KRPs*. Although *KRP5* is known as a positive regulator of endoreduplication in particular plant tissues such as in etiolated seedlings (Jégu *et al.* 2013; Wen *et al.* 2013), no clear stimulation of the endocycle was observed in GCs recorded by flow cytometry.

Giant cells overexpressing *KRP7* were significantly smaller, contained fewer nuclei that were larger and containing higher ploidy levels, and had less cytoplasm than in wild-type. Galls showed disordered cells neighbouring GCs compared to the wild-type. *KRP7* has been reported to be negatively regulated by BAF60, a subunit of SWI/SNF complexes of chromatin architecture remodelers. Plus, BAF60 is a positive regulator of

root development and cell cycle progression (Jégu *et al.* 2015). Although *KRP7* is normally not expressed within the GCs, its ectopic expression can induce severe changes in gall morphology, suggesting its capacity of de-regulation of CDK/CYC complexes occurring during gall ontogeny.

A noteworthy change in GC morphology was seen in *KRP3^{OE}* galls. Artificial *KRP3* expression caused an elongated GC phenotype with reduced cell size, already observed at early stages of gall development (7 DAI) compared to the large and rounded wild-type sectioned GCs. Regulatory mechanisms that control gall organization and GC shape involving the cell cycle are not yet reported and ectopic *KRP3* expression might regulate GC morphogenesis. As well, rearrangements of galls cells might influence the direction of GC expansion along the vascular cylinder. Plants overexpressing *KRP3* display reduced organ size, serrated leaves and reduced fertility, and show higher DNA ploidy level in the shoot apical meristem (SAM) and leaf tissues (Jun *et al.* 2013). Although DNA content increased in galls up to 128C ploidy levels and displayed a higher percentage of nuclei with prominent DNA content originated from GC, these did not enlarge. Our data strongly suggests that atypical *KRP3* expression in galls exerts a negative regulatory role in the mitotic cell cycle possibly provoked by the inhibition of CDK/CYC complexes anticipating endoreduplication, as seen for the SAM and leaves (Jun *et al.* 2013). This will compromise gall expansion affecting the nematode's life cycle with a strong decrease in progeny.

Aberrant nuclei morphology caused by the cumulative *KRP3* and *KRP5* expression in giant cells is possibly linked to their proteins nuclear localization patterns

Development of the NFS during RKN parasitism involves a tight regulation of both the mitotic and endoreduplication cycles (de Almeida Engler *et al.* 1999, 2012, 2015). Repeated endocycle events will result in duplicated chromatids that continue associated within a sole chromocenter (Comai 2005). Giant cell nuclei of *KRP1^{OE}*, *KRP4^{OE}* (Vieira *et al.* 2012, 2013), *KRP3^{OE}* and *KRP5^{OE}* lines showed subnuclear localization distribution in a spotted pattern that has been linked with

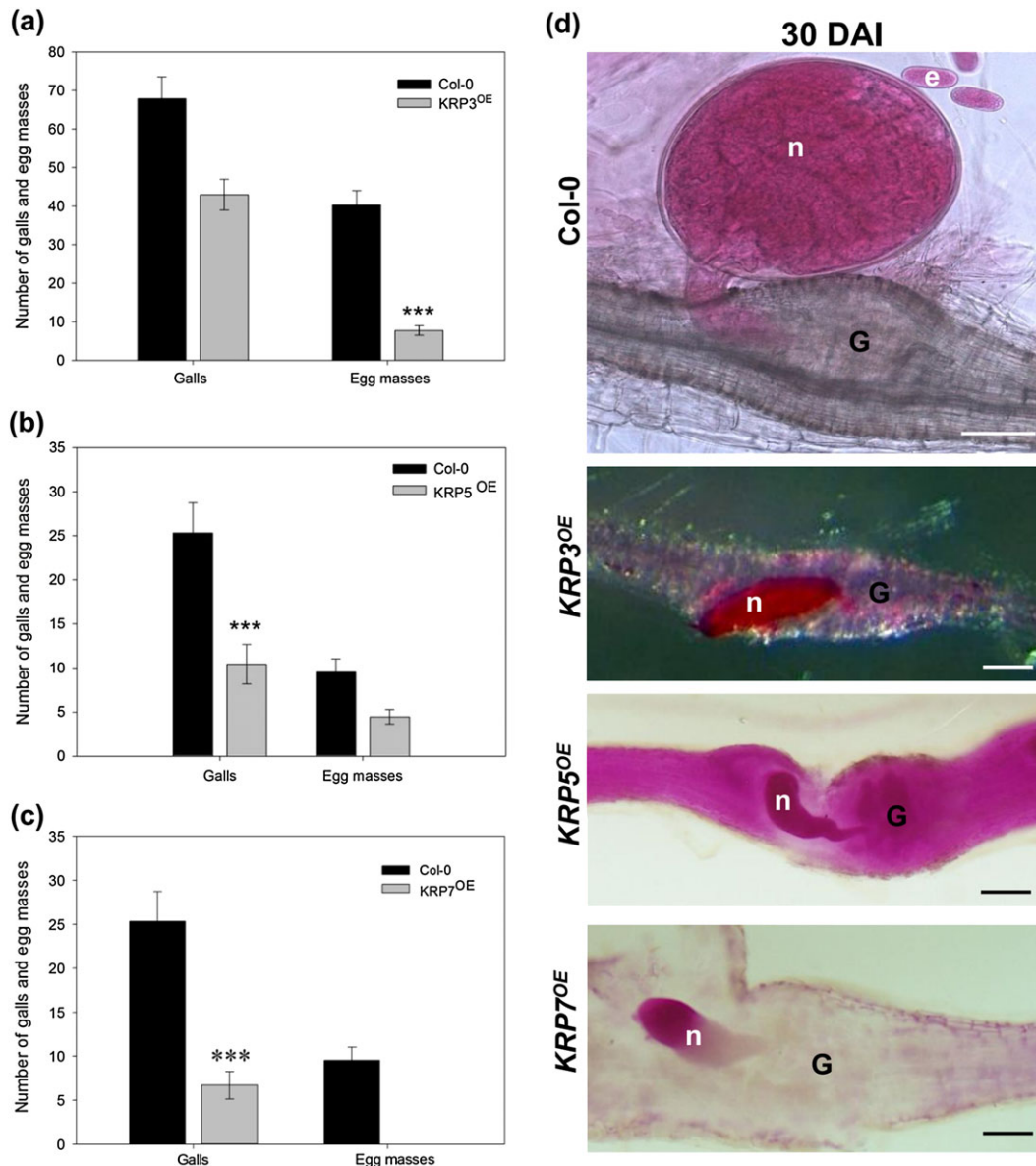


Figure 9. Nematode infection tests of *KRP3*, *KRP5* and *KRP7* overexpressing lines drastically affect nematode reproduction. (a) Nematode infection tests of the *KRP3*^{OE}, (b) *KRP5*^{OE} and (c) *KRP7*^{OE} lines compared to the wild-type. Data shown in (a–c) represent means \pm SD from two independent biological repetitions, in which a minimum of 30 seedlings of each line was evaluated for nematode infection. Pairwise comparisons were made by Student's *t*-test ($P \leq 0.001$). (d) Acid fuchsin staining of galls 30 DAI show that for all three overexpressing lines there is a delay or arrest in nematode development consequently inhibiting egg production. e, eggs; G, gall; n, nematode. Scale bars = 50 μ m.

chromocenters, and co-localized to chromosomes during mitosis (Jakoby *et al.* 2006; Bird *et al.* 2007; Jégu *et al.* 2013 and our work). Interestingly, their overexpression resulted in a convoluted and distended nuclear phenotype, caused by cumulative effect with gall aging, suggesting that excess of KRP protein in GCs deregulates mitosis possibly provoking an incorrect segregation of chromosome most likely enhanced by the high mitotic activity.

This might lead to nuclei enveloping more chromosomes than normally observed in GCs nuclei. Likewise, the excess binding of these KRPs upon overexpression in various loci of chromatin might affect heterochromatin structure.

Jégu *et al.* (2013) suggested *KRP5* as a multifunctional protein connecting transcriptional regulation of key cell cycle genes as well as modulating heterochromatin structure, because its overexpression decreases chromatin compaction and increases endoreduplication. Indeed, less compacted chromocenters were observed in GC nuclei of the *KRP5*^{OE} line, suggesting a link of this protein to have a function in heterochromatin structure allowing endoreduplication of regions that normally are not replicated.

Interestingly, *KRP1*, 3, 4 and 5 present a conserved nuclear localization signal motif (YLQLRSRRL) that is responsible for the spotted sub-localization in the nuclei (Jakoby *et al.*

2006; Zhou *et al.* 2006). Additionally, Nafati *et al.* (2010) identified a motif [LGVTR(A/K/R)(S/T)LAL] only present in KRP3, 4 and 5 also promoting the spotted sub-localization. This additional domain could explain why the punctate sub-localization of KRP3, 4 and 5 is more pronounced compared to KRP1, illustrated in Bird *et al.* (2007) and Vieira *et al.* (2012, 2013 and this work).

Differently, our previous and current studies have shown that KRP2, 6 and 7 proteins localize to the nucleoplasm in a homogeneous manner and never to chromosomes during mitosis as seen for KRP1, 3, 4 and 5 (Bird *et al.* 2007; Vieira *et al.* 2012, 2013, 2014). As well, that nuclei morphology in GCs is not connected but rather resembles the amoeboid like shape as in wild-type GCs (Vieira *et al.* 2013, 2014; and this work, respectively).

Treatment of *KRP5^{OE}* infected roots with a proteasome inhibitor suggests KRP5 protein accumulation in galls

KRP1, KRP2 and KRP3 regulate plant development and are regulated by 26S proteasome-mediated protein degradation being KRP6 targeted for degradation by specific E3 ligases (Zhou *et al.* 2003; Weinl *et al.* 2005; Jakoby *et al.* 2006; Liu *et al.* 2008; Ren *et al.* 2008; Jun *et al.* 2013). The F-box-like 17 complex formed by an SKP1-Cullin-F-box protein E3 ubiquitin ligase targets KRP members for proteasome-dependent degradation, as the loss of F-box-like 17 function leads to the stabilization of KRP members and inhibition of the cell cycle progress (Kim *et al.* 2008; Zhao *et al.* 2012). *In vivo* examination of uninfected and infected roots treated with the proteasome inhibitor MG132 showed enhanced GFP expression, suggesting that KRP5 protein levels accumulated in treated cell nuclei and is controlled by the proteasome. These observations suggest that KRP5 abundance via temporal protein degradation during gall development might be important for cell cycle regulation and consequently for nematode feeding site expansion and nematode reproduction.

In summary, the functional characterization performed herein of the three additional cell cycle inhibitor genes (*KRP3*, *KRP5* and *KRP7*) has highlighted interesting features of these *KRP* family members with respect to the other members of the *KRP* gene family previously investigated. Inhibiting KRP3 and KRP7 activity resulted in a more drastic decrease in gall size preventing nematode maturation. *KRP3* and *KRP7* genes are naturally not expressed in galls, and therefore ectopic expression of non- or weakly expressed *KRPs* might lead to the inactivation of CDKA/CYCD complexes disturbing progression of the cell cycle and thereby interfering with GC fate and nematode survival. Detailed analysis of the diverse members of the *KRP* multi-gene family gave us information of gene function, as well allowed us to select effective and robust inhibitor(s) suited for developing new strategies to decrease nematode propagation by inhibiting feeding site development. Since engineering forced expression of KRP inhibitors in GCs have been shown to be deleterious for gall development, this strategy can be considered as a potential approach for RKN control. On the whole, for this approach, KRP1, 2, 3, 4 and 7

seem to be best candidates for a gall-targeted ectopic expression. When a viable level of resistance in crop plants may be accomplished, this approach could be, extended towards other cell cycle-dependent nematode feeding sites as syncytia (de Almeida Engler *et al.* 1999, 2015; de Almeida Engler & Gheysen 2013) induced by cyst nematodes.

ACKNOWLEDGMENTS

We thank C. Escudero, M.Y. Serrano, I.M. Torres and F. E. Diaz Manzano for helping with *KRP* mutant analyses, Nathalie Marteu for providing pre-parasitic nematodes and Natalia Rodiuc for bulking seeds. We thank J. Boruc and E. Russinova for kindly providing primary transformants of *KRPs* overexpressing lines. R.C. has been supported by a doctoral scholarship in Brazil from CNPq (process number: 143030/2009-4) and in France from CAPES (process number: 6585-11-6), J. D.A.S.J. has been supported by a post doctoral scholarship of a CAPES-COFECUB (no. sv 683/10 2011) project.

REFERENCES

- Antonino de Souza Junior J.D., Grossi de Sa M.F., Engler G. & de Almeida Engler J. (2016) Imaging nuclear morphology and organization in cleared plant tissues treated with cell cycle inhibitors. In *Plant Cell Division: Methods and Protocols, Methods in Molecular Biology* (ed Caillaud M.C.), pp. 59–68. Science + Business Media, New York, USA.
- Beeckman T. & Engler G. (1994) An easy technique for the clearing of histochemically stained plant tissue. *Plant Molecular Biology Reporter* **12**, 37–42.
- Bird D.A., Buruiana M.M., Zhou Y., Fowke L.C. & Wang H. (2007) *Arabidopsis* cyclin dependent kinase inhibitors are nuclear-localized and show different localization patterns within the nucleoplasm. *Plant Cell Reports* **26**, 861–872.
- Boruc J., Van den Daele H., Hollunder J., Rombauts S., Mylle E., Hilson P., ... Russinova E. (2010) Functional modules in the *Arabidopsis* core cell cycle binary protein–protein interaction network. *Plant Cell* **22**, 1264–1280.
- Comai L. (2005) The advantages and disadvantages of being polyploid. *Nature Reviews Genetics* **6**, 836–846.
- de Almeida Engler J., De Vleeschauwer V., Burssens S., Celenza J.L., Inz D., Van Montagu M., ... Gheysen G. (1999) Molecular markers and cell cycle inhibitors show the importance of cell cycle progression in nematode-induced galls and syncytia. *Plant Cell* **11**, 793–807.
- de Almeida Engler J., Engler G. & Gheysen G. (2011) Unravelling the plant cell cycle in nematode induced feeding sites. In *Genomics and Molecular Genetics of Plant–Nematode Interactions* (eds Jones J., Gheysen G. & Fenoll C.), pp. 349–368. Science+Business Media, Dordrecht, the Netherlands.
- de Almeida Engler J. & Gheysen G. (2013) Nematode-induced endoreduplication in plant host cells: why and how? *Molecular Plant–Microbe Interactions* **26**, 17–24.
- de Almeida Engler J., Kyndt T., Vieira P., Van Cappelle E., Boudolf V., Sanchez V., ... Gheysen G. (2012) *CCS52* and *DELI* genes are key components of the endocycle in nematode-induced feeding sites. *The Plant Journal* **72**, 185–198.
- de Almeida Engler J., Vieira P., Rodiuc N., Grossi De Sa M.F. & Engler G. (2015) The plant cell cycle machinery: usurped and modulated by plant parasitic nematodes. *Advances in Botanical Research—Plant nematodes interactions*. In *Plant Nematode Interactions: A View on Compatible Interrelationships* (eds Escobar C. & Fenoll C.), pp. 91–118. ISBN:9780124171619.
- de Almeida Engler J., Siqueira K.M.S., Nascimento D.C., Costa T.G., Engler G. (2016). A cellular outlook of galls induced by root-knot nematodes in the model host *Arabidopsis thaliana*. *Nematoda* 6. ed. <http://dx.doi.org/10.4322/nematoda.00616>.
- De Veylder L., Beeckman T., Beemster G.T., Krols L., Terras F., Landrieu I., ... Inzé D. (2001) Functional analysis of cyclin-dependent kinase inhibitors of *Arabidopsis*. *Plant Cell* **13**, 1653–1668.
- De Veylder L., Beeckman T. & Inzé D. (2007) The ins and outs of the plant cell cycle. *Nature Reviews Molecular Cell Biology* **8**, 655–665.
- Gheysen G. & Fenoll C. (2002) Gene expression in nematode feeding sites. *Annual Review of Phytopathology* **40**, 191–219.

- Hoth S., Stadler R., Sauer N. & Hammes U.Z. (2008) Differential vascularization of nematode-induced feeding sites. *Proceedings of the National Academy of Sciences of the United States of America* **105**, 12617–12622.
- Huang C.S. (1985) Formation, anatomy and physiology of giant cells induced by root-knot nematodes. In *An Advanced Treatise on Meloidogyne* (eds Barker K. R., Carter C.C. & Sasser J.N.), pp. 223. Department of Plant Pathology and US Agency for International Development, Raleigh, North Carolina.
- Inze D. & De Veylder L. (2006) Cell cycle regulation in plant development. *Annual Review of Genetics* **40**, 77–105.
- Jakoby M.J., Weinel C., Pusch S., Kuijt S.J., Merkle T., Dissmeyer N. & Schnittger A. (2006) Analysis of the subcellular localization, function, and proteolytic control of the *Arabidopsis* cyclin dependent kinase inhibitor ICK1/KRP1. *Plant Physiology* **141**, 1293–1305.
- Jégu T., Domenichini S., Blein T., Ariel F., Christ A., Kim S.K., ... Benhamed M. (2015) A SWI/SNF chromatin remodelling protein controls cytokinin production through the regulation of chromatin architecture. *PLoS ONE* **10**, e0138276.
- Jégu T., Latrasse D., Delarue M., Mazubert C., Bourge M., Hudik E., ... Benhamed M. (2013) Multiple functions of KRP5 connect endoreduplication 25 and cell elongation. *Plant Physiology* **16**, 11694–11705.
- Jones M.G.K. & Northcote D.H. (1972) Multinucleate transfer cells induced in coleus roots by the root-knot nematode, *Meloidogyne arenaria*. *Protoplasma* **75**, 381–395.
- Jun S., Okushima Y., Nam J., Umeda M. & Kim G.-T. (2013) Kip-related protein 3 is required for control of endoreduplication in the shoot apical meristem and leaves of *Arabidopsis*. *Molecules and Cells* **35**, 47–53.
- Karimi M., Inzé D. & Depicker A. (2002) “GATEWAY” vectors for *Agrobacterium*-mediated plant transformation. *Trends in Plant Science* **7**, 193–195.
- Kim H.J., Oh S.A., Brownfield L., Hong S.H., Ryu H., Hwang I., ... Nam H.G. (2008) Control of plant germline proliferation by SCF^{FBL17} degradation of cell cycle inhibitors. *Nature* **455**, 1134–1137.
- Liu J., Zhang Y., Qin G., Tsuge T., Sakaguchi N., Luo G., ... Qu L.-J. (2008) Targeted degradation of the cyclin-dependent kinase inhibitor ICK4/KRP6 by RINGtype E3 ligase is essential for mitotic cell cycle progression during *Arabidopsis* gametogenesis. *Plant Cell* **20**, 1538–1554.
- Menges M., de Jager S.M., Gruissem W. & Murray J.A. (2005) Global analysis of the core cell cycle regulators of *Arabidopsis* identifies novel genes, reveals multiple and highly specific profiles of expression and provides a coherent model for plant cell cycle control. *The Plant Journal* **41**, 546–566.
- Menges M. & Murray J.A. (2002) Synchronous *Arabidopsis* suspension cultures for analysis of cell-cycle gene activity. *The Plant Journal* **30**, 203–212.
- Moens M., Perry R.N. & Starr J.L. (2009) *Meloidogyne* species—a diverse group of novel and important plant parasites. In *Root-Knot Nematodes* (eds Perry R. N., Moens M. & Starr J.L.), pp. 1–17. CABI, Wallingford, UK.
- Nafati M., Frangne N., Hernould M., Chevalier C. & Gévaudant F. (2010) Functional characterization of the tomato cyclin-dependent kinase inhibitor SIKRP1 domains involved in protein–protein interactions. *New Phytologist* **188**, 136–149.
- Niebel A., de Almeida Engler J., Hemery A., Ferreira P., Van Montagu M. & Gheysen G. (1996) Induction of *cdc2a* and *cyclA1* expression in *Arabidopsis* during early phases of nematode-induced feeding cell formation. *The Plant Journal* **10**, 1037–1043.
- Ormenese S., de Almeida Engler J., De Groodt R., De Veylder L., Inze D. & Jacquard A. (2004) Analysis of the spatial expression pattern of seven Kip related proteins (KRPs) in the shoot apex of *Arabidopsis thaliana*. *Annals of Botany* **93**, 575–580.
- Ren H., Santner A., de Pozo J.C., Murray J.A.H. & Estelle M. (2008) Degradation of the cyclin-dependent kinase inhibitor KRP1 is regulated by two different ubiquitin E3 ligase. *The Plant Journal* **53**, 705–716.
- Rodiuc N., Vieira P., Banora M.Y. & de Almeida Engler J. (2014) On the track of transfer cell formation by specialized plant-parasitic nematodes. *Frontiers in Plant Science* **5**, 160.
- Rutter W.B., Hewezi T., Abubucker S., Maier T.R., Huang G., Mitreva M., ... Baum T.J. (2014) Mining novel effector proteins from the esophageal gland cells of *Meloidogyne incognita*. *Molecular Plant–Microbe Interactions* **27**, 965–974.
- Sijmons P.C., Atkinson H.J. & Wyss U. (1994) Parasitic strategies of root nematodes and associated host cell responses. *Annual Review of Phytopathology* **32**, 235–259.
- Sijmons P.C., Grundler F.M.W., Vonmende N., Burrows P.R. & Wyss U. (1991) *Arabidopsis thaliana* as a new model host for plant-parasitic nematodes. *Plant Journal* **1**, 245–254.
- Van Leene J., Boruc J., De Jaeger G., Russinova E. & De Veylder L. (2011) A kaleidoscopic view of the *Arabidopsis* core cell cycle interactome. *Trends in Plant Science* **16**, 141–150.
- Van Leene J., Hollunder J., Eeckhout D., Persiau G., Van De Slijke E., Stals H., ... De Jaeger G. (2010) Targeted interactomics reveals a complex core cell cycle machinery in *Arabidopsis thaliana*. *Molecular Systems Biology* **6**, 397.
- Verkest A., Weinel C., Inzé D., De Veylder L. & Schnittger A. (2005) Switching the cell cycle. Kip-related proteins in plant cell cycle control. *Plant Physiology* **139**, 1099–1106.
- Vieira P. & de Almeida Engler J. (2015) The plant cell inhibitor KRP6 is involved in multinucleation and cytokinesis disruption in giant-feeding cells induced by root-knot nematode. *Plant Signaling and Behavior* **10**, e1010924.
- Vieira P., De Clercq A., Stals H., Van Leene J., Van De Slijke E., Van Isterdael G., ... de Almeida Engler J. (2014) The cyclin-dependent kinase inhibitor KRP6 induces mitosis and impairs cytokinesis in giant cells induced by plant-parasitic nematodes in *Arabidopsis*. *Plant Cell* **26**, 2633–2647.
- Vieira P., Engler G. & de Almeida Engler J. (2012) Whole-mount confocal imaging of nuclei in giant feeding cells induced by root-knot nematodes in *Arabidopsis*. *New Phytologist* **195**, 488–496.
- Vieira P., Escudero C., Rodiuc N., Boruc J., Russinova E., Glab N., ... de Almeida Engler J. (2013) Ectopic expression of Kip-related proteins restrains root-knot nematode-feeding site expansion. *New Phytologist* **199**, 505–519.
- Wang H., Fowke L.C. & Crosby W.L. (1997) A plant cyclin-dependent kinase inhibitor gene. *Nature* **386**, 451–452.
- Wang H., Zhou Y. & Fowke L.C. (2006) The emerging importance of cyclin-dependent kinase inhibitors in the regulation of the plant cell cycle and related processes. *Canadian Journal of Botany* **84**, 640–650.
- Weinel C., Marquardt S., Kuijt S., Nowack M., Jakoby M., Hülskamp M. & Schnittger A. (2005) Novel functions of plant cyclin-dependent kinase inhibitors, ICK1/KRP1, can act non-cell autonomously and inhibit entry into mitosis. *Plant Cell* **17**, 1704–1722.
- Wen B., Nieuwland J. & Murray J.A. (2013) The *Arabidopsis* CDK inhibitor ICK3/KRP5 is rate limiting for primary root growth and promotes growth through cell elongation and endoreduplication. *Journal of Experimental Botany* **64**, 1135–1144.
- Zhang L., Davies L.J. & Elling A.A. (2015) A *Meloidogyne incognita* effector is imported into the nucleus and exhibits transcriptional activation activity in planta. *Molecular Plant Pathology* **16**, 48–60.
- Zhao X.-A., Harashima H., Dissmeyer N., Pusch S., Weimer A.K., Bramsiepe J., ... Schnittger A. (2012) A general G1/S-phase cell-cycle control module in the flowering plant *Arabidopsis thaliana*. *PLoS Genetics* **8**, e1002847.
- Zhou Y., Li G., Brandizzi F., Fowke L.C. & Wang H. (2003) The plant cyclin-dependent kinase inhibitor ICK1 has distinct functional domains for *in vivo* kinase inhibition, protein instability and nuclear localization. *The Plant Journal* **35**, 476–489.
- Zhou Y., Niu H., Brandizzi F., Fowke L.C. & Wang H. (2006) Molecular control of nuclear and subnuclear targeting of the plant CDK inhibitor ICK1 and ICK1-mediated nuclear transport of CDKA. *Plant Molecular Biology* **62**, 261–278.

Received 30 March 2016; accepted for publication 6 January 2017

SUPPORTING INFORMATION

Additional Supporting Information may be found in the online version of this article at the publisher's web-site:

Figure S1. Expression pattern of three *KRPpro:GUS* lines in galls of *Arabidopsis* roots infected with *M. incognita*. Promoter activity of *KRP3*, *KRP5* and *KRP7* during gall development (3, 7, 14 and 21 d after inoculation). Dark-field images illustrate GUS staining in red. White lines underlie the nematode induced giant-feeding cells. Asterisk, giant cell; n, nematode; NC, neighbouring cells. Scale bars = 50 µm.

Figure S2. Characterization of *Arabidopsis krp5* loss of function lines. (a) PCR analyses of single T-DNA insertions (SALK_053533 and SALK_089717) into the *KRP5* gene. (b) RT-PCR performed with specific primers showing the absence of full-length transcripts of *krp5* loss of function lines.

Figure S3. KRP overexpressing lines used for *M. incognita* inoculation assays. (a) Phenotype of wild-type (Col-0) plants

compared to *KRP3^{OE}*, *KRP5^{OE}* and *KRP7^{OE}* lines. (b) Transcript levels of *KRP^{OE}* lines were examined by RT-PCR-based DNA gel blot analysis, showing highest transcript levels in the *KRP3^{OE}* and *KRP7^{OE}* lines. (c) Nuclear localization of KRP3, KRP5 and KRP7 in *Arabidopsis* root cells. For both KRP3 and KRP5, a sub-nuclear localization is also observed. (d) Root apical meristems in *KRP3*, *KRP5* and *KRP7* overexpressing *Arabidopsis* roots are apparently smaller than in wild-type. Scale bars = 50 μm .

Figure S4. Giant cell surface (μm^2) measurements of wild-type plants compared to the *KRP* overexpressing lines at different stages after nematode infection (7, 14, 21 and 40 DAI). Measurements were made on a minimum of 30 giant cell sections (only the two to three largest giant cells were measured per gall) for *KRP3^{OE}* (a) and *KRP5^{OE}* (b), while for *KRP7^{OE}* (c) measurements were only performed for 21 DAI. Letters 'a' and 'b' represent significant difference of 5% of probability for each time point.

Figure S5. *In vivo* localization of (a,b) KRP3-GFP and (c,d) KRP7-GFP in nuclei of galls induced by *M. incognita*. KRP3-GFP showed grouped and interconnected nuclei within giant cells (arrows). Scale bars = 25 μm .

Figure S6. Nuclear flow cytometry analyses of uninfected roots of *KRP* overexpressing lines compared to wild-type. Representative flow cytometry graphics of nuclei isolated from 4-week-old roots (approximately 2000 nuclei were measured per run). (a) *KRP3^{OE}*, (b) *KRP5^{OE}*, (c) *KRP7^{OE}*.

Table S1. List of primers used.

Movie S1. 3D confocal projections of serial optical sections of a 21-day-old gall induced by *M. incognita* in the *KRP3^{OE}* line.

Movie S2. 3D confocal projections of serial optical sections of a 21-day-old gall induced by *M. incognita* in the *KRP5^{OE}* line.

Movie S3. 3D confocal projections of serial optical sections of a 21-day-old gall induced by *M. incognita* in the *KRP7^{OE}* line.

Movie S4. 3D confocal projections of serial optical sections of a 21-day-old gall induced by *M. incognita* in the wild-type.